THE JOURNAL OF PHYSICAL CHEMISTRY A

Article

pubs.acs.org/JPCA

Ultrafast Dissociation Dynamics of 2-Ethylpyrrole

Neil C. Cole-Filipiak,[†] Michael Staniforth,[†,‡] Natércia d. N. Rodrigues,[†] Yoann Peperstraete,[§] and Vasilios G. Stavros*[,†]

[†]Department of Chemistry, University of Warwick, Library Road, Coventry CV4 7AL, United Kingdom

[‡]Department of Physics, University of Warwick, Gibbet Hill Road, Coventry CV4 7AL, United Kingdom

[§]AILES beamline, L'Orme des Merisiers, Synchrotron SOLEIL, Saint Aubin, BP 48, 91192 Gif sur Yvette Cedex, France

S *Supporting Information*

ABSTRACT: To explore the effects of ring substitution on dissociation dynamics, the primary photochemistry of 2-ethylpyrrole was explored using ultrafast ion imaging techniques. Photoexcitation to the S_1 state, a $\pi\sigma^*$ state, in the range from 238 to 265 nm results in cleavage of the N−H bond with an H atom appearance lifetime of ca. 70 fs. The insensitivity of this lifetime to photon energy, combined with a small kinetic isotope effect, suggests that tunneling does not play a major role in N−H bond cleavage. Total kinetic energy release spectra reveal modest vibrational excitation in the radical counter-fragment, increasing with photon energy. At wavelengths less than or equal to 248 nm, an additional low kinetic energy H atom loss mechanism becomes available with an appearance lifetime of ∼1.5 ps, possibly due to the population of higher-lying $^1\pi\pi^*$ states.

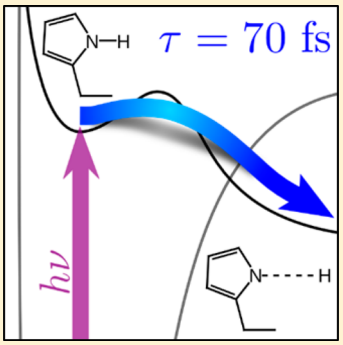

I. INTRODUCTION

The photochemistry and photophysics of biopolymers is of fundamental interest to chemists and biologists seeking to understand the photostability of life's essential molecules. In an effort to understand the photochemistry of these complicated systems,[1] the dynamics of the underlying subunits are investigated[2−4] with increasing molecular complexity. This "bottom-up" approach allows molecular structure−function−property relationships to be systematically explored (see, e.g., refs 5−7). Recently, the photochemistry of aromatic heterocycles (e.g., phenol and pyrrole) that form the principal building blocks of diverse biological polymers has attracted the interest of spectroscopists.[2,8] Of particular interest are the $\sigma^*\leftarrow\pi$ electronic transitions present in these heterocycles.[4] Photoexcitation to these states may result in several photoproducts (see, e.g., ref 9) including the prompt loss of hydrogen atoms,[4] a dissociation mechanism of potential relevance in biochemistry[10] and crucial to understanding the ubiquitous presence of these photolabile biomolecules.

As the basic subunit of diverse biomolecules such as tryptophan or heme,[11,12] the photodissociation of the aromatic heterocycle pyrrole (c-C_4H_5N) from the S_1 ($^1\pi\sigma^*$) state has been extensively studied with a majority of studies focusing on the rapid N−H bond fission.[13−16] Utilizing a variety of time-resolved techniques, several groups have investigated the ultrafast excited-state dynamics via time-resolved ion yield (TR-IY) of the pyrrole cation,[17−19] photoelectron spectroscopy,[20,21] or H atom elimination from pyrrole[17,22] with some of the most recent work exploring the excited-state dynamics of pyrrole dimers.[23,24] The electronic structure and dissociation dynamics have also been extensively modeled theoretically with the most recent work focusing on the choice of initial conditions[25] and the role of tunneling[26−28] during H atom loss. From these efforts, it is clear that the S_1 state of pyrrole has an ∼0.2 eV barrier along the N−H stretch coordinate, followed by a repulsive potential leading to the production of photoproducts (predominantly) in the electronic ground state. After photoexcitation to the S_1 state below the barrier, the H atom appearance lifetime is ∼130 fs; the same excitation in deuterated pyrrole yields a kinetic isotope effect (KIE) of 11.[22] When the photon energy places excited-state population above the barrier, the H atom appearance lifetime decreases to ∼50 fs with a KIE of 3.[22] Both theory and experiment have concluded that this dramatic decrease in both H atom appearance lifetime and KIE demonstrate the importance of tunneling dynamics during pyrrole photodissociation.[22,26]

To move toward larger biological systems, the effects of ring substitution on the photochemistry of the N−H bond in pyrrole must be explored. As demonstrated with phenol, another prototypical biological chromophore, ring substitution can have a substantial effect on a molecule's primary photochemistry and photophysics (see, e.g., refs 29 and 30), including the dynamics of H atom loss. Recently, a combination of experimental and theoretical investigations by Ashfold and co-workers explored the effects of pyrrole-ring functionalization upon energy partitioning (i.e., internal vs kinetic) during N−H bond fission in 2,5-dimethylpyrrole (2,5-DMP),[31] 2,4-dimethylpyrrole (2,4-DMP),[32] and 2-ethylpyrrole (2-EP).[32] Using

Received: December 5, 2016
Revised: January 9, 2017
Published: January 10, 2017

DOI: 10.1021/acs.jpca.6b12228
J. Phys. Chem. A 2017, 121, 969−976

high-energy resolution H Rydberg atom photofragment translational spectroscopy (HRA-PTS), the group showed that the addition of alkyl groups to the ring lowered the N−H bond dissociation energy relative to bare pyrrole. Supported by calculations, the observed total kinetic energy release (TKER) spectra also revealed substituent-dependent vibrational excitation in the radical photoproducts due to Franck−Condon and molecular symmetry considerations.[32]

Continuing the work of Karsili et al.,[32] another study used time-resolved velocity map imaging (TR-VMI) to probe H atom loss from 2,4-DMP.[33] In contrast to the H atom appearance lifetimes from pyrrole dissociation,[22] the lifetime from 2,4-DMP dissociation (ca. 120 fs) was insensitive to photon energy. A modest KIE, also in contrast to pyrrole, revealed that tunneling apparently plays a minor role in H atom loss from 2,4-DMP. These results support the interpretation that the one-dimensional N−H bond stretch coordinate is insufficient to describe H atom loss from 2,4-DMP. Rather, the methyl groups open reaction coordinates "around" the barrier resulting in an effectively barrierless dissociation. Recent work on the time-resolved photoelectron spectroscopy of 2,5-DMP also concluded that photoexcited population likely does not encounter a barrier as it leaves the S_1 vertical Franck−Condon (vFC) region.[34]

In the present work, we expand upon previous investigations[32,33] by examining the time-resolved dissociation dynamics of H atom loss from the S_1 state of 2-EP (see Figure 1 for structure and UV absorption spectrum). Though 2-EP is a structural isomer of 2,4-DMP, we find a further shortening of the H atom appearance lifetime that is again insensitive to photon energy. Our results will be discussed with regard to structural and possible excited-state potential energy surface (PES) differences.

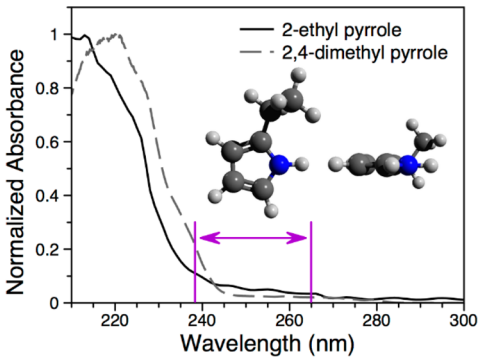

Figure 1. Vapor-phase ultraviolet absorption spectra of 2-EP (solid line) and 2,4-DMP (dashed line, ref 33). The lines indicate the wavelength range investigated in the present study. (inset) Top and side views of 2-EP in the S_0 equilibrium geometry (based on calculations in ref 32).

II. METHODS

Experiments were performed using a TR-VMI apparatus previously described in detail.[33,35,36] 2-EP (Fischer Scientific, 98%) was filtered through neutral alumina to remove contaminants prior to use; the purity was confirmed by ^{1}H NMR. A molecular beam of 2-EP was produced by flowing ∼3 bar of He over a reservoir of sample (refreshed daily) heated to ∼35 °C. The resulting gas mixture was then expanded into vacuum by an Even-Lavie pulsed solenoid valve[37] operating at 125 Hz. The beam passes through a 2 mm skimmer that serves to separate the source and interaction chambers. In the interaction chamber, the beam is intersected by two temporally delayed femtosecond ultraviolet (UV) laser pulses (see below) that initiate photochemistry (the "pump") and ionize (the "probe") the resulting photoproducts. Ions are accelerated down a time-of-flight tube by a set of ion optics based upon the design of Eppink and Parker.[38] The accelerated ions impact upon an imaging stack, consisting of pair of microchannel plates coupled to a phosphor screen (Photek, VID-240), and the resulting images are recorded by a CCD camera (Basler, A-312f) interfaced with a computer. Temporal gating of the detector electronics allow for the exclusive detection of H^+ (or D^+) ions.

To produce the pump and probe light, 800 nm laser pulses of ∼40 fs duration are produced by a commercial Ti:sapphire oscillator and regenerative amplifier system (Spectra-Physics Tsunami and Spitfire XP) operating at 1 kHz. This fundamental beam is split and used to pump two tunable UV optical parametric amplifiers (Light Conversion, TOPAS-C) producing the two UV pulses. The pump pulse was tuned over the wavelength range of λ_{pump} = 238 nm (42 020 cm^{-1}, the shortest TOPAS wavelength) to 265 nm (37 740 cm^{-1}, the approximate onset of $S_1 \leftarrow S_0$ absorption in 2-EP), indicated as lines in Figure 1. The probe pulse is centered at λ_{probe} = 243 nm (41 150 cm^{-1}) to provide 2 + 1 resonance enhanced multiphoton ionization (REMPI) of H atom photofragments via the two-photon allowed 2s←1s transition (82 259.158 cm^{-1}). The pump pulse is temporally delayed with respect to the probe pulse (Δt) by a hollow corner gold retroreflector mounted on a motorized delay stage, resulting in a maximum temporal delay of Δt = 1.2 ns. The laser beams are focused to intersect the molecular beam within the ion optics, with the electric fields of both laser pulses parallel to the plane of the imaging stack. The design and electric potentials of the ion optics and detector projects the three-dimensional photofragment velocity distribution onto the two-dimensional imaging detector, resulting in a VMI.[38]

TR-IY studies were also performed on select ions. Here, a digital oscilloscope (LeCroy LT372 Waverunner) monitors the current impacting the phosphor screen as a function of ion time-of-flight (TOF) since the interaction of the laser and molecular beams. For consistency with the imaging experiments, the electric fields of both lasers were parallel to the plane of the imaging stack. TR-IY transients were produced by integrating ion counts at specific m/z values—or, for the H^+ transients, integrating regions of the TKER spectrum—as a function of Δt. Characterization of the instrument response function (IRF) at temporal overlap of the pump and probe pulses (Δt = 0) was performed via TR-IY of Xe^+. The resulting transient, an example of which is shown in the Supporting Information, was fit to a Gaussian distribution with a full width at half-maximum (fwhm) of ∼100 fs, yielding a maximum temporal resolution of ca. 30 fs.

Deuterated 2-EP (d_1-EP) was produced by stirring freshly filtered 2-EP with d_4-methanol for ∼48 h under anhydrous, inert atmosphere. The solvent was then removed by fractional distillation under vacuum (0.5 mbar, 25−45 °C temperature gradient), while the product was collected over ice (ca. 4 °C) and stored under inert atmosphere prior to use. H/D exchange was inferred by the reduction of ^{1}H NMR signal at the hydride position, indicating the formation of a N−D bond. The TOF

DOI: 10.1021/acs.jpca.6b12228
J. Phys. Chem. A 2017, 121, 969−976

mass spectrum showed approximately equal amounts of the 2-EP and d_1-EP parent molecular ions.

One-color, 243 nm "probe alone" images were subtracted from each pump−probe image; negligible H^+ signal was produced by the pump laser. Experiments performed with an off-resonance probe (e.g., 245 nm) produced negligible H^+ signal. Pump laser power studies were conducted at several wavelengths. In all cases, the recorded signal showed a linear dependence on pump laser power, consistent with one-photon photoexcitation. To explore the signal dependence upon molecular beam characteristics, H^+ transients were also taken at the shortest pump wavelengths using 4 bar of Ar to back the pulsed valve. In addition to the time-resolved studies, the static UV absorption spectrum of vapor-phase 2-EP, shown in Figure 1, was acquired using a Cary 60 UV/vis spectro-photometer by placing a drop of room-temperature 2-EP into an empty quartz cuvette.

III. RESULTS AND ANALYSIS

From the VMI, the original three-dimensional photofragment velocity distribution was reconstructed and integrated using the polar onion peeling (POP) method,[39] resulting in the one-dimensional photofragment velocity and angular distributions. After calibrating to the known dissociation energetics of HBr at 200 nm,[40] the velocity distribution may be transformed into a one-dimensional total kinetic energy release (TKER) spectrum. By conservation of energy, TKER spectra yield information about a two-body dissociation event through the following relationship:

$$\mathrm{TKER} + E_{\mathrm{int}} = hc/\lambda_{\mathrm{pump}} - D_0 + E_0 \quad (1)$$

where TKER is the total kinetic energy of the system, E_{int} is the total internal energy of the photofragments (which, for H atom loss, may be assumed to be exclusively in the molecular cofragment), $hc/\lambda_{\mathrm{pump}}$ is the pump photon energy, D_0 is the asymptotic bond dissociation energy, and E_0 is the internal energy of the 2-EP molecule prior to photoexcitation. During POP deconvolution, the reconstructed photofragment angular distributions are fit to the known functional form[41] and may be characterized by an anisotropy parameter β. For a single photon initiated photodissociation event, the anisotropy parameter provides a measure of the alignment between the transition dipole moment and dissociation vector, taking the limiting values of −1 or 2 corresponding to perpendicular or parallel transitions, respectively; a value of $\beta = 0$ corresponds to an isotropic angular distribution.

a. TKER Spectra. Example TKER spectra of H atom loss from 2-EP are shown in Figure 2. Additional spectra at other pump wavelengths may be found in the Supporting Information; details of all TKER spectra may be found in Table 1. In the limit of internally cold molecules (i.e., $E_{\mathrm{int}} = E_0 = 0$) the maximum available kinetic energy $\mathrm{TKER}_{\mathrm{max}}$ is calculated using a N−H bond dissociation energy of 31 650 cm^{-1} (ref 32) and is indicated on each spectrum as an arrow. The TKER spectra show a clear shift in peak intensity from $\mathrm{TKER}_{\mathrm{max}}$ at the longest pump wavelength to ∼2000 cm^{-1} below $\mathrm{TKER}_{\mathrm{max}}$ as the pump wavelength is decreased to 248 nm, resulting in a nearly constant 6000−7000 cm^{-1} high KE feature. While the spectra in Figure 2 lack vibrational structure, the peak positions and qualitative shapes are in excellent agreement with the previously reported HRA-PTS spectra.[32] For $\lambda_{\mathrm{pump}} > 248$ nm (examples shown in Figure 2a,b), there is

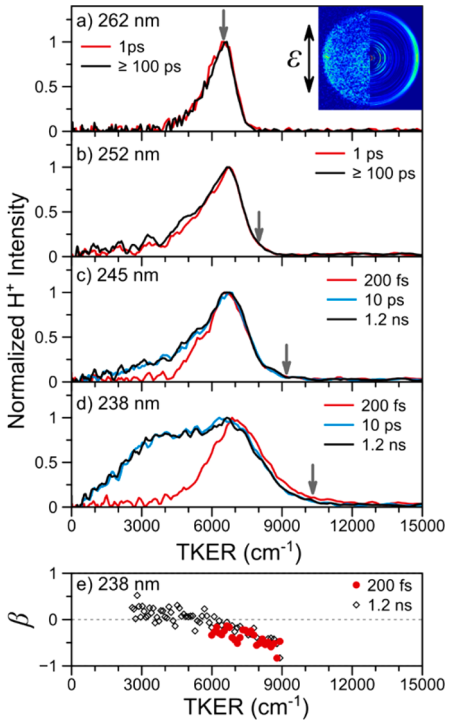

Figure 2. Example TKER spectra for pump wavelengths (a) 262, (b) 252, (c) 245, and (d) 238 nm at several time delays (Δt, indicated in the figure). The arrows indicate $\mathrm{TKER}_{\mathrm{max}}$ using the results of Karsili et al.[32] (e) Anisotropy parameter β as a function of TKER for the indicated time delays at 238 nm. (inset) Subtracted (left) and deconvoluted (right) VMI image recorded at 262 nm. The arrow indicates the electric field vector of the laser pulses.

Table 1. TKER Spectral Information and H-Atom (or D-Atom) Appearance Lifetimes for 2-EP

pump wavelength (nm)	$\mathrm{TKER}_{\mathrm{max}}$ (cm^{-1})	peak TKER (cm^{-1})	anisotropy parameter	H atom appearance lifetime (fs)
265	6090	6000	−0.6	70 ± 20
262	6520	6600	−0.5	55 ± 13
257	7260	6200	−0.5	60 ± 30
252	8030	6800	−0.5	70 ± 20
248	8670	6600	−0.6	80 ± 20
245, high KE	9170	6600	−0.5	68 ± 10
245, low KE	–[a]	∼4000	–	1600 ± 600
241, high KE	9844	6700	−0.5	76 ± 10
241, low KE	–	∼4000	0.05	1600 ± 200
238, high KE	10370	6900	−0.4	70 ± 20
238, low KE	–	∼4000	0.07	1520 ± 120
257 (D atom)	–	5300	−0.4	140 ± 20

[a]–, unknown quantity or low signal-to-noise ratio.

no apparent difference between TKER spectra acquired at Δt = 1 ps or ≥100 ps, suggesting that N−H bond fission is complete within the first picosecond. The measured photofragment angular distributions yield an anisotropy parameter of $-0.6 \leq \beta \leq -0.4$ for all pump wavelengths investigated, again in agreement with the HRA-PTS result of $\beta \approx -0.6$.[32] The constant anisotropy parameter of 2-EP is in contrast with H atom loss from 2,4-DMP, which showed an increasing value of β toward 0 as the pump photon energy was increased.[33]

In addition to a high KE feature at ∼7000 cm^{-1}, at $\lambda_{\mathrm{pump}} \leq$ 248 nm a second TKER feature appears centered at ∼4000

DOI: 10.1021/acs.jpca.6b12228
J. Phys. Chem. A 2017, 121, 969−976

cm^{-1} (see Figure 2c,d). Absent at a time delay of Δt = 200 fs, this low KE feature remains unchanged for time delays $\Delta t \geq 10$ ps. At Δt = 200 fs, the TKER peak position and anisotropy parameter of $\beta \approx -0.5$ are consistent with the values determined at all other pump wavelengths, suggesting that the high KE feature is due to the same dissociation mechanism as occurs at longer pump wavelengths. For $\Delta t \geq 10$ ps, the value of β at low KE appears to be slightly positive (as shown in Figures 2e and S2), resulting in an average $\beta \approx 0$ across the entire TKER spectrum.

b. H Atom Appearance Lifetimes. To measure the H atom appearance lifetimes, TKER spectra were recorded at numerous time delays Δt. The entire TKER feature, ~3000−9000 cm^{-1} depending on the pump wavelength, was then integrated as a function of time delay to produce H^+ transients, as shown in the examples in Figure 3 (additional H^+ transients

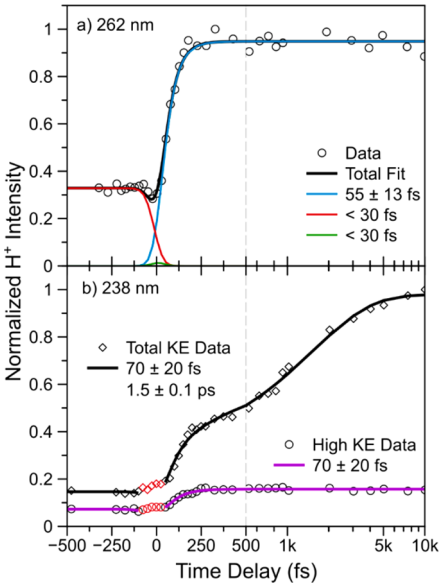

Figure 3. Integrated TKER signal intensity as a function of time delay following photoexcitation at (a) 262 nm and (b) 238 nm. Data are shown as black points; excluded data (due to additional reverse dynamics) are shown in red. Fits to the data are shown as solid lines with "breaks" to account for the excluded data. At 262 nm, individual components and associated time constants of the fit are shown as blue (forward time), red (reverse time), and green (multiphoton dynamics near Δt = 0); see Supporting Information for further details. The time axis was corrected to place Δt = 0 at t_0^{true}. The gray, dashed line marks the change from a linear to logarithmic time axis.

may be found in the Supporting Information). To extract the appearance lifetimes, these transient data were fit with a kinetic model assuming exponential rises in H^+ signal in forward (Δt > 0) and reverse (Δt < 0) time, as well as an exponential decay near Δt = 0, convoluted with a Gaussian IRF; further descriptions and details of the kinetic model may be found in the Supporting Information and refs 17, 22, and 33. For all transients, the precise location of Δt = 0 (t_0^{true}, see Supporting Information for details) was determined using either the integrated, multiphoton H^+ signal (TKER > 15 000 cm^{-1}) or the TR-IY of Xe^+.

Results from the H^+ transients are summarized in Table 1; reported errors are the standard error from the fit. For pump wavelengths longer than 245 nm, the entire TKER spectra show an average H atom appearance lifetime of ca. 70 fs regardless of pump photon energy. For $\lambda_{pump} \leq 245$ nm, integration of the high KE portion of the TKER spectra (~7000−10 000 cm^{-1}) as a function of time delay results in similar H atom appearance lifetimes. H^+ transients from $\lambda_{pump} \leq 245$ nm have an additional temporal component due to the low KE TKER feature. At these short wavelengths, fits to the total transients—with fixed short time behavior from the high KE fits—return an average low KE appearance lifetime of ~1.5 ps. While the TKER spectrum acquired at λ_{pump} = 248 nm and Δt > 1 ps shows a slight intensity increase at low KE (see Figure S1), attempts to fit the 248 nm H^+ transient including a second appearance lifetime were inconclusive. At 238 nm—shown in Figure 3b—additional "reverse" (i.e. probe initiated) dynamics appear in the H^+ transient and, as such, data near Δt = 0 were excluded from the fit.

c. Deuterated 2-EP Results. Similar to the TKER spectra and H^+ transients shown in Figures 2 and 3, a TKER spectrum and D^+ transient from the photodissociation of d_1-EP at λ_{pump} = 257 nm are shown in Figure 4. The TKER spectrum is peaked

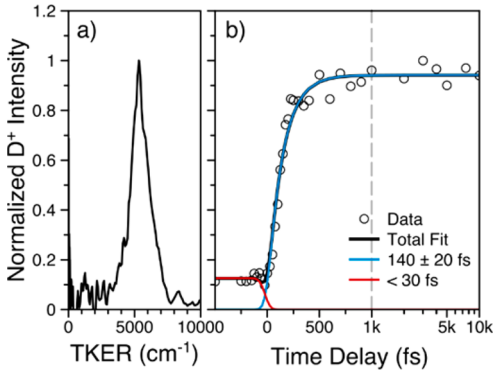

Figure 4. (a) TKER spectrum and (b) D^+ transient from the photodissociation of d_1-EP at λ_{pump} = 257 nm. For the transient, data are shown as open circles, and the total kinetic fit is shown in black. Individual components and associated time constants of the fit are shown as blue (forward time) and red (reverse time). The gray, dashed line marks the change from a linear to logarithmic time axis. The time axis was not corrected with t_0^{true}.

at 5450 cm^{-1}, ~800 cm^{-1} less than the peak TKER value in the corresponding H atom spectrum (due to the differences in the zero-point energies of the vibrational modes lost during the dissociation) and in agreement with the trends observed from the HRA-PTS study of d_5-pyrrole.[42] Using the same kinetic model as above, the best fit to the D^+ transient data shown in Figure 4b yields a D atom appearance lifetime of 140 ± 20 fs, which, when compared to the average H atom appearance lifetime, yields a KIE ≈ 2. TKER spectra from d_1-EP at λ_{pump} = 238 nm are shown in the Supporting Information. Similar to the spectra shown in Figure 2d, a second, low KE feature appears at longer time delays.

d. Time-Resolved Ion Yield Transients. Example TR-IY transients for the 2-EP parent molecular ion (m/z = 95) at 252 and 238 nm are shown in the Supporting Information. These transients were fit with a kinetic model assuming exponential decays, in both forward and reverse time, convoluted with a Gaussian IRF function; further details of this kinetic model may also be found in the Supporting Information. At 252 nm, the 2-EP parent ion shows an increase in signal at Δt = 0, followed by an ultrafast decay with a 66 ± 14 fs lifetime, similar to the behavior of 2,5-DMP.[34] At 238 nm, an additional decay lifetime

DOI: 10.1021/acs.jpca.6b12228
J. Phys. Chem. A 2017, 121, 969−976

is needed to produce a satisfactory fit, yielding τ_1 < 30 fs (i.e., below the temporal resolution of the experiment) and τ_2 = 970 ± 80 fs.

IV. DISCUSSION

For pump wavelengths longer than 245 nm, the TKER spectra, angular distributions, and spectral onset of the $S_1 \leftarrow S_0$ transition in 2-EP are all consistent with distributions and trends from the HRA-PTS study by Karsili et al.[32] At the lowest photon energy studied, the TKER feature is peaked at the $TKER_{max}$ assuming N−H bond fission; higher pump photon energies merely result in increased vibrational excitation of the C_6H_8N radical cofragment and a relatively constant peak TKER feature. The portion of the main TKER feature greater than $TKER_{max}$ is largely due to the broadband laser pulse (ca. 500 cm^{-1} fwhm). While H atom loss from the α carbon of the ethyl group is energetically feasible at 265 nm—assuming a similar dissociation energy to the corresponding C−H bond in ethylbenzene[43]—the resulting $TKER_{max}$ would be ∼7900 cm^{-1}, well above the observed peak at 6000 cm^{-1} in the experimental TKER spectrum. Finally, the appearance of similar D atom results of the photodissociation of d_1-EP suggest that N−H cleavage is responsible for the observed H atom signal. Given the above evidence, N−H bond fission to produce the 2-ethylpyrrol-1-yl radical (2-EPyl) is thus the most likely dissociation mechanism, and the observed dynamics may be interpreted as such.

Fits to the H atom transients recorded at λ_{pump} > 245 nm (and the high KE H atoms at $\lambda_{pump} \leq$ 245 nm) all return a H atom appearance lifetime of ∼70 fs, similar to pyrrole photodissociation above the S_1 barrier (50 fs)[22] and consistent with ultrafast dissociation along a repulsive excited-state surface. However, the measured lifetime is shorter than either 2,4-DMP[33] (120 fs) or pyrrole photoexcited below the barrier (130 fs). In addition to the short appearance lifetime, the invariance of the lifetime with photon energy and the modest KIE ≈ 2 suggest that the broadband laser pulse creates an excited-state wavepacket favorably placed for rapid, barrier-free N−H bond fission, similar to the dissociation of 2,4-DMP.[33] The agreement between the H atom appearance lifetime and the 2-EP^+ transient decay lifetime at λ_{pump} = 252 nm suggests that, at longer wavelengths, N−H bond cleavage may be the primary decay pathway out of the vFC region. Two possible, and not exclusive, scenarios to explain this behavior become readily apparent. In the first scenario, the barrier along the N−H stretch coordinate is quite small, and, given the ∼500 cm^{-1} bandwidth of the pump laser, these experiments would thus be insensitive to said barrier. Alternatively, the reaction coordinate for H atom loss—not exclusively the N−H stretch—may not have a significant barrier to dissociation. Though details of the S_1 surface along the N−H stretch coordinate in 2-EP have not been published, the negligible barrier in the first scenario seems unlikely, as the S_1 well depth in pyrrole *increases* with alkyl substitution.[22,26,32,34] Given that previous studies of 2,4-DMP[33] and 2,5-DMP[34] both concluded that tunneling plays a minor role in the S_1 state dynamics and dissociation, the latter scenario seems more likely to apply to 2-EP. Ultimately, dynamical calculations upon the 2-EP S_1 potential energy surface would be of significant interest to help determine the route to dissociation.

While it is tempting to attribute the shortening of the lifetime to the difference in the density of states between 2,4-DMP and 2-EP, this explanation does not address the difference in angular distribution behavior (for 2,4-DMP, β approaches 0 with increasing photon energy,[33] while, for 2-EP, β remains constant). Rather, the different behaviors of these isomers may be due to the reduction in symmetry, C_s for 2,4-DMP versus C_1 for 2-EP, which will result in a greater number of dipole allowed electronic transitions in 2-EP (namely, the $\sigma^* \leftarrow \pi$ transition to the S_1 state). Qualitatively, the effects of molecular symmetry may be seen in Figure 1, where the long wavelength absorption in 2-EP is approximately twice as intense (relative to the strong $\pi^* \leftarrow \pi$ transitions at shorter wavelengths) as the same feature in 2,4-DMP. In the case of the more symmetric 2,4-DMP, the increase in β toward 0 was attributed to vibronic enhancement of the $S_1 \leftarrow S_0$ transition with higher-lying, allowed $\pi^* \leftarrow \pi$ transitions. While similar mixing may be occurring in 2-EP, the allowed transition to the S_1 state may reduce the relative importance of any "mixed" excitations and thus preserve the H atom angular distribution at all wavelengths. However, further work (such as the H atom appearance lifetime from the dissociation of 2,5-DMP) will be needed to explore the effects of molecular symmetry and ring substitution on pyrrole dissociation in greater detail.

Similar to the results from 2,4-DMP dissociation,[33] an additional feature appears at low KE in the TKER spectra for $\lambda_{pump} \leq$ 248 nm (exemplified in Figure 2c,d). As can be seen in Figure 2e and Figure S2 in the Supporting Information, the low KE feature has a small positive value of β, in marked contrast with the high KE value of $\beta = -0.5$ and similar to the value of $\beta \approx 0$ from the 2,4-DMP low KE H atom angular distribution.[33] Given the differences in the KE and angular distributions, and that the H atom appearance lifetime for this low KE feature is substantially longer (1.5 ps) than the high KE feature, an additional dissociation mechanism must be invoked for this signal. To evaluate the possible dissociation mechanisms, we must first consider the source of these low KE H atoms. As previously established for 2,4-DMP, assignment of this spectral feature to clusters in the molecular beam may be eliminated based on several factors, including: the minimal cluster signal in the observed TOF spectrum; the low concentration, less than 0.5%,[44] of 2-EP in the molecular beam; and the insensitivity of the low KE feature to choice of backing gas (see Methods), stagnation pressure, or other molecular beam parameters. Additionally, as mentioned in Section II, the use of a fresh 2-EP sample every day minimizes the possibility that this feature is due to a contaminating species. Karsili et al.[32] also report a modest increase in the low KE portion of the HRA-PTS TKER spectrum with a 246 nm pump wavelength, further supporting the assignment of this low KE feature to the dissociation of 2-EP. The similar low KE feature seen in the TKER from d_1-EP at λ_{pump} = 238 nm (see Supporting Information) strongly indicates that the low KE H atoms are due to cleavage of the hydride bond in 2-EP. As a final note, attribution of the near-zero value of β to rotational motion of 2-EP prior to dissociation is unlikely given the short H atom appearance lifetime of 1.5 ps.

With the assignment of these low KE H atoms to N−H bond fission, we can conclude that the 2-EPyl radical internal energy must be greater and this dissociation mechanism must either (i) produce electronically excited 2-EPyl radical or (ii) involve coupling to a greater number of vibrational modes than the ultrafast dissociation from the S_1 state. The overlapping TKER features make a firm assignment of $TKER_{max}$, and thus the 2-EPyl radical internal energy, impossible. It is thus unclear whether these low KE H atoms are due to decay along the S_1 or

DOI: 10.1021/acs.jpca.6b12228
J. Phys. Chem. A 2017, 121, 969−976

another higher-energy surface, possibly similar to the S_2 ($^1\pi\sigma^*$) surface of 2,4-DMP.[33] Because of the similarity of 2,4-DMP and 2-EP, the 2-EPyl radical D_1 state is expected to lie ~7000 cm^{-1} above the D_0 state,[33] which would limit $TKER_{max}$ for this channel to ~3000 cm^{-1}, slightly below the peak of the observed low KE feature. Though it cannot be entirely eliminated, possibility (i) thus seems unlikely given the observed energetics.

With situation (ii), we must address why the population of additional vibrational modes has a distinct spectral onset and is coincident with an elongation of the dissociation lifetime. The appearance of the low KE feature could be related to population of higher-lying electronic excited states with an absorption onset of ~245 nm, in reasonable agreement with the static absorption spectrum shown in Figure 1 and consistent with the excited-state dynamics of 2,5-DMP.[34] Assuming that the dissociation produces 2-EPyl in the ground electronic state (see Discussion above), the population initially excited to S_n (where n denotes one or more excited states lying above S_1) must undergo internal conversion (IC) to the S_1 state followed by dissociation to produce ground electronic state 2-EPyl. Indeed, the similarity of the low KE appearance lifetime (1.5 ps) with the second decay lifetime from the 2-EP parent ion transient (~1 ps) suggests that migration out of the vFC region—for example, via IC—may be the rate-limiting step to dissociation at these wavelengths. It is important to note that other, excited-state de-excitation pathways may contribute to the difference between the two lifetimes (a detail that may also explain the shortening of the 2-EP^+ sub-picosecond decay lifetime as λ_{pump} is decreased). As with pyrrole, the shift in TKER could be due to the involvement of high-energy C−H vibrational and ring-stretching modes during IC,[45] with vibrational excitation retained in the 2-EPyl radical cofragment after dissociation. Recent theoretical work by Shalashilin and co-workers on the dynamics of H atom loss from pyrrole[27] found several trajectories, involving contributions from higher-lying excited states, that eject low KE H atoms. Furthermore, H atoms from these trajectories were ejected perpendicular to the molecular plane and, assuming the same transition dipole moment as the $S_1 \leftarrow S_0$ transition, would thus result in $\beta \geq 0$. While relatively few trajectories showed this behavior, the calculated photoexcitation was essentially "at threshold," meaning that these pathways may become more important at higher excitation energies. It thus seems reasonable to conclude that the low KE H atoms with a small, positive anisotropy parameter observed herein are due to population of higher-lying electronic excited states of 2-EP. If IC is involved in the low KE dissociation mechanism, we would expect the low KE appearance lifetime to decrease with increasing photon energy. Unfortunately, this trend cannot be evaluated due to the limited number of, and uncertainty in, the reported lifetimes (see Table 1).

To close the discussion of the low KE feature, we note that while fits to the high KE transients for $\lambda_{pump} \leq 245$ nm remain acceptable (see Figure S4 in the Supporting Information), the quality of the total H^+ transient fits decreases with decreasing pump wavelength. This decrease in fit quality, particularly near $\Delta t = 0$ (see Figure S7 in the Supporting Information), may be due to a breakdown of the assumption of parallel dynamics. Indeed, if population in a higher-lying excited state must first decay to another state (e.g., S_1) prior to dissociation, then a sequential kinetic model would be a more appropriate description of these low KE H atoms.[46] However, a more rigorous analysis of this low KE feature is beyond the scope of the present investigation of photodissociation from the S_1 state of 2-EP.

Finally, as discussed in the Supporting Information, the TKER spectrum derived from the m/z = 80 photofragment is likely due to cleavage of the C−C bond within the ethyl group, producing a CH_3 radical and a benzyl radical-like C_5H_6N species (2-methylene pyrrole radical). A low average KE, along with an appearance lifetime of much greater than 1.2 ns for the m/z = 80 fragment, suggests that this channel is due to dissociation on the ground electronic state after vibrational energy randomization. As a rise in the m/z = 80 signal is only observed at 238 nm, CH_3 loss is either a minor decay channel or is only accessible with higher photon energies.

V. CONCLUSIONS

We have shown that in the wavelength range from 238 to 265 nm, photoexcitation to the S_1 state of 2-EP results in ultrafast H atom loss. TKER spectra show increasing 2-EPyl vibrational excitation with increasing pump photon energy, consistent with the previous HRA-PTS study on this system.[32] The H^+ transients reveal an H atom appearance lifetime of ~70 fs, consistent with prompt dissociation along a repulsive surface. The insensitivity of this appearance lifetime to pump photon energy and the modest KIE suggest that the H atom loss coordinate is effectively barrierless. At the shortest wavelengths studied, a second, low KE feature appears in the TKER spectra with a lifetime of 1.5 ps, which is tentatively assigned to H atom loss following population of higher-lying singlet states. At the shortest wavelength studied, evidence for ground-state CH_3 loss was also found.

Along with the previous studies of 2-EP,[32] 2,4-DMP,[32,33] and 2,5-DMP,[31,34] the results from the present investigation further support the following trend: the addition of alkyl groups to the aromatic ring provides a route "around" the excited-state barrier along the N−H stretch coordinate, resulting in a net decrease in H atom appearance lifetime. The symmetry of the molecule may play an important role in the dissociation, and additional insights may be gained by exploring the effects of different substituents on the ring. Thus, while subtle changes in the structure of C_6H_9N have an impact on the excited-state dynamics (e.g., the reduction in H atom appearance lifetime), the global photodynamics of these molecules apparently remains relatively constant as molecular complexity is increased. Importantly, this work reinforces the importance of systematic exploration of the structure−function−property triad; mapping and understanding these changes is essential for a complete "bottom-up" elucidation of the photochemistry of pyrrole-based biomolecules.

■ ASSOCIATED CONTENT

Supporting Information

The Supporting Information is available free of charge on the ACS Publications website at DOI: 10.1021/acs.jpca.6b12228.

All data underpinning the present work are published in the supporting information. This includes, additional TKER spectra, VMI recorded at 238 nm, details of the IRF and kinetic models, additional H^+ transients, d_1-EP TKER spectra at 238 nm, 2-EP^+ TR-IY transients, a detailed view of the 238 nm H^+ transients, and the m/z = 80 TR-IY transient and TKER spectrum. (PDF)

DOI: 10.1021/acs.jpca.6b12228
J. Phys. Chem. A 2017, 121, 969−976

AUTHOR INFORMATION

Corresponding Author

*E-mail: v.stavros@warwick.ac.uk. Phone: +44 (0)24731 50172.

ORCID

Neil C. Cole-Filipiak: 0000-0002-3619-8915

Notes

The authors declare no competing financial interest.

ACKNOWLEDGMENTS

The authors would like to thank W.-D. Quan for assistance with 2-EP purification and deuteration, H. L. Wainwright and S. Trouton for laboratory assistance, and the group of Prof. D. Shalashilin for productive conversations. N.C.C.F. thanks the Leverhulme Trust for postdoctoral research funding; M.S. thanks the EPSRC for funding; N.d.N.R. thanks the EPSRC for doctoral funding; Y.P. thanks the Ecole Normale Supérieure Paris-Saclay for doctoral funding. V.G.S. thanks the EPSRC for an equipment grant (EP/J007153) and the Royal Society for a University Research Fellowship.

REFERENCES

(1) Creed, D. The photophysics and photochemistry of the near-UV absorbing amino acids − I. Tryptophan and its simple derivatives. *Photochem. Photobiol.* **1984**, *39*, 537−562.

(2) Roberts, G. M.; Stavros, V. G. The role of $\pi\sigma^*$ states in the photochemistry of heteroaromatic biomolecules and their subunits: insights from gas-phase femtosecond spectroscopy. *Chem. Sci.* **2014**, *5*, 1698−1722.

(3) Staniforth, M.; Stavros, V. G. Recent advances in experimental techniques to probe fast excited-state dynamics in biological molecules in the gas phase: dynamics in nucleotides, amino acids and beyond. *Proc. R. Soc. London, Ser. A* **2013**, *469*, 2013045810.1098/rspa.2013.0458

(4) Ashfold, M. N. R.; King, G. A.; Murdock, D.; Nix, M. G. D.; Oliver, T. A. A.; Sage, A. G. $\pi\sigma^*$ excited states in molecular photochemistry. *Phys. Chem. Chem. Phys.* **2010**, *12*, 1218−1238.

(5) Chatterley, A. S.; Young, J. D.; Townsend, D.; Zurek, J. M.; Paterson, M. J.; Roberts, G. M.; Stavros, V. G. Manipulating dynamics with chemical structure: probing vibrationally-enhanced tunnelling in photoexcited catechol. *Phys. Chem. Chem. Phys.* **2013**, *15*, 6879−6892.

(6) Dixon, R. N.; Oliver, T. A. A.; Ashfold, M. N. R. Tunnelling under a conical intersection: Application to the product vibrational state distributions in the UV photodissociation of phenols. *J. Chem. Phys.* **2011**, *134*, 194303.

(7) Oliver, T. A. A.; King, G. A.; Ashfold, M. N. R. Position matters: competing O-H and N-H photodissociation pathways in hydroxy- and methoxy-substituted indoles. *Phys. Chem. Chem. Phys.* **2011**, *13*, 14646−14662.

(8) Sobolewski, A. L.; Domcke, W.; Dedonder-Lardeux, C.; Jouvet, C. Excited-state hydrogen detachment and hydrogen transfer driven by repulsive $^1\pi\sigma^*$ states: A new paradigm for nonradiative decay in aromatic biomolecules. *Phys. Chem. Chem. Phys.* **2002**, *4*, 1093−1100.

(9) Blank, D. A.; North, S. W.; Lee, Y. T. The ultraviolet photodissociation dynamics of pyrrole. *Chem. Phys.* **1994**, *187*, 35−47.

(10) Kohen, A.; Klinman, J. P. Hydrogen tunneling in biology. *Chem. Biol.* **1999**, *6*, R191−R198.

(11) Fenna, R.; Zeng, J.; Davey, C. Structure of the green heme in myeloperoxidase. *Arch. Biochem. Biophys.* **1995**, *316*, 653−656.

(12) Walsh, C. T.; Garneau-Tsodikova, S.; Howard-Jones, A. R. Biological formation of pyrroles: Nature's logic and enzymatic machinery. *Nat. Prod. Rep.* **2006**, *23*, 517−531.

(13) Wei, J.; Kuczmann, A.; Riedel, J.; Renth, F.; Temps, F. Photofragment velocity map imaging of H atom elimination in the first excited state of pyrrole. *Phys. Chem. Chem. Phys.* **2003**, *5*, 315−320.

(14) Cronin, B.; Nix, M. G. D.; Qadiri, R. H.; Ashfold, M. N. R. High resolution photofragment translational spectroscopy studies of the near ultraviolet photolysis of pyrrole. *Phys. Chem. Chem. Phys.* **2004**, *6*, 5031−5041.

(15) Wei, J.; Riedel, J.; Kuczmann, A.; Renth, F.; Temps, F. Photodissociation dynamics of pyrrole: Evidence for mode specific dynamics from conical intersections. *Faraday Discuss.* **2004**, *127*, 267−282.

(16) Rubio-Lago, L.; Zaouris, D.; Sakellariou, Y.; Sofikitis, D.; Kitsopoulos, T. N.; Wang, F.; Yang, X.; Cronin, B.; Devine, A. L.; King, G. A.; et al. Photofragment slice imaging studies of pyrrole and the Xe···pyrrole cluster. *J. Chem. Phys.* **2007**, *127*, 064306.

(17) Lippert, H.; Ritze, H. H.; Hertel, I. V.; Radloff, W. Femtosecond time-resolved hydrogen-atom elimination from photoexcited pyrrole molecules. *ChemPhysChem* **2004**, *5*, 1423−1427.

(18) Montero, R.; Peralta Conde, Á.; Ovejas, V.; Fernández-Fernández, M.; Castaño, F.; Vázquez de Aldana, J. R.; Longarte, A. Femtosecond evolution of the pyrrole molecule excited in the near part of its UV spectrum. *J. Chem. Phys.* **2012**, *137*, 064317.

(19) Montero, R.; Ovejas, V.; Fernández-Fernández, M.; Peralta Conde, Á.; Longarte, A. Revisiting the relaxation dynamics of isolated pyrrole. *J. Chem. Phys.* **2014**, *141*, 014303.

(20) Wu, G.; Neville, S. P.; Schalk, O.; Sekikawa, T.; Ashfold, M. N. R.; Worth, G. A.; Stolow, A. Excited state non-adiabatic dynamics of pyrrole: A time-resolved photoelectron spectroscopy and quantum dynamics study. *J. Chem. Phys.* **2015**, *142*, 074302.

(21) Crane, S. W.; Zawadzki, M. M.; Thompson, J. O. F.; Kotsina, N.; Ghafur, O.; Townsend, D. Caveats in the interpretation of time-resolved photoionization measurements: A photoelectron imaging study of pyrrole. *J. Chem. Phys.* **2016**, *145*, 234304.

(22) Roberts, G. M.; Williams, C. A.; Yu, H.; Chatterley, A. S.; Young, J. D.; Ullrich, S.; Stavros, V. G. Probing ultrafast dynamics in photoexcited pyrrole: Timescales for $^1\pi\sigma^*$ mediated H-atom elimination. *Faraday Discuss.* **2013**, *163*, 95−116.

(23) Montero, R.; León, I.; Fernández, J. A.; Longarte, A. Femtosecond Excited State Dynamics of Size Selected Neutral Molecular Clusters. *J. Phys. Chem. Lett.* **2016**, *7*, 2797−2802.

(24) Neville, S. P.; Kirkby, O. M.; Kaltsoyannis, N.; Worth, G. A.; Fielding, H. H. Identification of a new electron-transfer relaxation pathway in photoexcited pyrrole dimers. *Nat. Commun.* **2016**, *7*, 11357.

(25) Barbatti, M.; Sen, K. Effects of different initial condition samplings on photodynamics and spectrum of pyrrole. *Int. J. Quantum Chem.* **2016**, *116*, 762−771.

(26) Sapunar, M.; Ponzi, A.; Chaiwongwattana, S.; Malis, M.; Prlj, A.; Decleva, P.; Doslic, N. Timescales of N-H bond dissociation in pyrrole: a nonadiabatic dynamics study. *Phys. Chem. Chem. Phys.* **2015**, *17*, 19012−19020.

(27) Makhov, D. V.; Saita, K.; Martinez, T. J.; Shalashilin, D. V. Ab initio multiple cloning simulations of pyrrole photodissociation: TKER spectra and velocity map imaging. *Phys. Chem. Chem. Phys.* **2015**, *17*, 3316−3325.

(28) Makhov, D. V.; Martinez, T. J.; Shalashilin, D. V. Toward fully quantum modelling of ultrafast photodissociation imaging experiments. Treating tunnelling in the ab initio multiple cloning approach. *Faraday Discuss.* **2016**, *194*, 81.

(29) Karsili, T. N. V.; Wenge, A. M.; Harris, S. J.; Murdock, D.; Harvey, J. N.; Dixon, R. N.; Ashfold, M. N. R. O-H bond fission in 4-substituted phenols: S_1 state predissociation viewed in a Hammett-like framework. *Chem. Sci.* **2013**, *4*, 2434−2446.

(30) Karsili, T. N. V.; Wenge, A. M.; Marchetti, B.; Ashfold, M. N. R. Symmetry matters: photodissociation dynamics of symmetrically versus asymmetrically substituted phenols. *Phys. Chem. Chem. Phys.* **2014**, *16*, 588−598.

(31) Cronin, B.; Nix, M. G. D.; Devine, A. L.; Dixon, R. N.; Ashfold, M. N. R. High resolution photofragment translational spectroscopy studies of the near ultraviolet photolysis of 2,5-dimethylpyrrole. *Phys. Chem. Chem. Phys.* **2006**, *8*, 599−612.

DOI: 10.1021/acs.jpca.6b12228
J. Phys. Chem. A 2017, 121, 969−976

(32) Karsili, T. N. V.; Marchetti, B.; Moca, R.; Ashfold, M. N. R. UV photodissociation of pyrroles: Symmetry and substituent effects. *J. Phys. Chem. A* **2013**, *117*, 12067−12074.
(33) Staniforth, M.; Young, J. D.; Cole, D. R.; Karsili, T. N. V.; Ashfold, M. N. R.; Stavros, V. G. Ultrafast excited-state dynamics of 2,4-dimethylpyrrole. *J. Phys. Chem. A* **2014**, *118*, 10909−10918.
(34) Ovejas, V.; Montero, R.; Fernández-Fernández, M.; Longarte, A. Tracking the relaxation of 2,5-dimethylpyrrole by femtosecond time-resolved photoelectron and photoion detection. *J. Phys. Chem. A* **2015**, *119*, 3355−3365.
(35) Iqbal, A.; Pegg, L.-J.; Stavros, V. G. Direct versus indirect H atom elimination from photoexcited phenol molecules. *J. Phys. Chem. A* **2008**, *112*, 9531−9534.
(36) Wells, K. L.; Perriam, G.; Stavros, V. G. Time-resolved velocity map ion imaging study of NH_3 photodissociation. *J. Chem. Phys.* **2009**, *130*, 074308.
(37) Even, U.; Jortner, J.; Noy, D.; Lavie, N.; Cossart-Magos, C. Cooling of large molecules below 1 K and He clusters formation. *J. Chem. Phys.* **2000**, *112*, 8068−8071.
(38) Eppink, A. T. J. B.; Parker, D. H. Velocity map imaging of ions and electrons using electrostatic lenses: Application in photoelectron and photofragment ion imaging of molecular oxygen. *Rev. Sci. Instrum.* **1997**, *68*, 3477−3484.
(39) Roberts, G. M.; Nixon, J. L.; Lecointre, J.; Wrede, E.; Verlet, J. R. R. Toward real-time charged-particle image reconstruction using polar onion-peeling. *Rev. Sci. Instrum.* **2009**, *80*, 053104.
(40) Regan, P. M.; Langford, S. R.; Orr-Ewing, A. J.; Ashfold, M. N. R. The ultraviolet photodissociation dynamics of hydrogen bromide. *J. Chem. Phys.* **1999**, *110*, 281−288.
(41) Zare, R. N. Photoejection dynamics. *Mol. Photochem.* **1972**, *4*, 1−37.
(42) Cronin, B.; Devine, A. L.; Nix, M. G. D.; Ashfold, M. N. R. Near ultraviolet photolysis of deuterated pyrrole. *Phys. Chem. Chem. Phys.* **2006**, *8*, 3440−3445.
(43) Luo, Y.-R. *Handbook of Bond Dissociation Energies in Organic Compounds;* CRC Press: 2002.
(44) Garrido, D. O. A.; Buldain, G.; Frydman, B. 1,4-Diaminoalkanes from pyrroles. A new synthetic approach to substituted putrescines. *J. Org. Chem.* **1984**, *49*, 2619−2622.
(45) Neville, S. P.; Worth, G. A. A reinterpretation of the electronic spectrum of pyrrole: A quantum dynamics study. *J. Chem. Phys.* **2014**, *140*, 034317.
(46) Chatterley, A. S.; Roberts, G. M.; Stavros, V. G. Timescales for adiabatic photodissociation dynamics from the Ã state of ammonia. *J. Chem. Phys.* **2013**, *139*, 034318.

DOI: 10.1021/acs.jpca.6b12228
J. Phys. Chem. A 2017, 121, 969−976